Food & Function

Enhancement of DPP-IV Inhibitory Activity and Capacity of Enabling GLP-1 Secretion Through RADA16-assisted Molecular Designed Rapeseed Peptide Nanogels

Journal:	*Food & Function*
Manuscript ID	FO-ART-12-2021-004367.R2
Article Type:	Paper
Date Submitted by the Author:	15-Mar-2022
Complete List of Authors:	Xu, Feiran; Hefei University of Technology, School of Food and Biological Engineering Xu, Baocai; Hefei University of Technology, School of Food and Biological Engineering Chen, Hong; University of Illinois at Urbana-Champaign Ju, Xingrong; Jiangnan University, National Engineering Laboratory for Cereal Fermentation Technology, State Key Laboratory of Food Science and Technology, School of Food Science and Technology Gonzalez de Mejia, Elvira; University of Illinois at Urbana-Champaign Department of Food Science and Human Nutrition, ;

Enhancement of DPP-IV Inhibitory Activity and Capacity of Enabling GLP-1 Secretion Through RADA16-assisted Molecular Designed Rapeseed Peptide Nanogels

Feiran Xu[1, 2]; Baocai Xu[1]; Hong Chen[2]; Xingrong Ju[3]; Elvira Gonzalez de Mejia[2]*

1. Engineering Research Center of Bio-process, Ministry of Education, School of Food and Biological Engineering, Hefei University of Technology, Hefei, 230009, People's Republic of China.

2. Department of Food Science and Human Nutrition, Division of Nutritional Sciences, University of Illinois at Urbana-Champaign, 228 Edward R. Madigan Laboratory (ERML), 1201 West Gregory Drive, Urbana, Illinois 61801, United States.

3. National Engineering Laboratory for Cereal Fermentation Technology, State Key Laboratory of Food Science and Technology, School of Food Science and Technology, Jiangnan University, Wuxi, 214122, People's Republic of China.

*Corresponding author:

Elvira Gonzalez de Mejia, Email: edemejia@illinois.edu;

Abstract: The potential of pentapeptide IPQVS (RAP1) and octopeptide ELHQEEPL (RAP2) derived from rapeseed napin as natural dipeptidyl-peptidase IV (DPP-IV) inhibitors is promising. The objective was to develop a nanogel strategy to resist the hydrolysis of digestive and intestinal enzymes, to enhance the DPP-IV inhibitory activity of RAP1 and RAP2, and stimulate glucagon-like peptide 1 (GLP-1) secretion of RAP2 by RADA16-assisted molecular design. The linker of double Gly was used in the connection of RADA16 and the functional oligopeptide region (RAP1 and RAP2). Compared to the original oligopeptides, DPP-IV IC_{50} of the nanogels RADA16-RAP1 and RADA16-RAP2 decreased by 26.43% and 17.46% in Caco-2 cell monolayers, respectively. The results showed that the two nanogel peptides with no toxicity to cells had higher content of stable β-sheet structures (increased by 5.6-fold and 5.2-fold, respectively) than the original oligopeptides, and self-assembled fibrous morphology. Rheological results suggested that the nanogels RADA16-RAP1 and RADA16-RAP2 exhibit good rheological properties for potential injectable applications; storage modulus (G') was 10 times higher than low modulus (G''). Furthermore, the RAP2 and its RADA16-assisted nanogel peptide at the concentration of 250 μM significantly ($P<0.05$) increased the release of GLP-1 by 35.46% through the calcium-sensing receptor pathway in the enteroendocrine STC-1 cells. Hence, the innovated and harmless nanogel with the sequence of RADA16-GG-X_n have the possibility of oral and injection for treating or relieving type 2 diabetes.

Key words: Rapeseed derived nanogel peptides; RADA16; DPP-IV inhibitory effects;

GLP-1 release; Caco-2 cell monolayers; STC-1 cells; CaSR pathway.

1. Introduction

Glucagon-like peptide-1 (GLP-1) is an endocrine hormone studied to have excellent insulinotropic actions, which is regarded as an effective candidate for the treatment or management of type 2 diabetes (T2D).[1] The rapid degradation of GLP-1 caused by dipeptidyl peptidase-IV (DPP-IV) occurs in organs or intestinal epithelium.[2] Therefore, the promotion of GLP-1 levels by inhibiting DPP-IV has obtained increasing attention.[3] It has been reported that zein[4], rice protein hydrolysate[5], and casein[6] had a dual mechanism in hypoglycemic action, which not only inhibited DPP-IV, but also increased the release of GLP-1.

DPP-IV inhibitory peptides RAP1 (IC_{50}= 52.16 μM) and RAP2 (IC_{50}= 78.46 μM) were proven to have excellent activity in the biochemical substrate-enzyme reaction system. However intestinal enzymes are not negligible factors restricting their actual function as confirmed by the Caco-2 cell monolayer experiment.[2, 7] RAP1 and RAP2 may stimulate the GLP-1 secretion through the mechanism that is analogous to the calcium-sensing receptor (CaSR) agonist peptides, including γ-Glu-Val-Gly[8], soybean tridecanoic peptide (β51–63)[9], and protamine polypeptide.[10] CaSR is a G-protein coupled receptor that are known to regulate hormone secretion including GLP-1 in the intestinal endocrine cells.[11] Human enteroendocrine cells (EECs), including L cells, are difficult to study because they only account for about 1% of intestinal epithelium.[12] In contrast, the mouse intestinal endocrine cells are relatively mature, such as STC-1 cells, which can be used in the study of GLP-1 release.[13]

Nevertheless, due to the influence of digestive enzymes and extreme pH, it is difficult for DPP-IV inhibitory or CaSR agonist peptides to play the role of enhancing GLP-1 activity in the surface of intestinal epithelial cells.[7, 14] Finding a suitable nano-delivery method is currently a difficult problem to be solved. Ion-complementary peptide that have Arg-Ala-Asp-Ala as a circulating sequence have been used in the study of gelatinous nano-delivery of active peptides.[15] For instance, a peptide hydrogel was developed by using RADA32 peptide with anticancer and immune-stimulating capabilities;[16] other researchers have reported a new RADA16-based nanogels to improve the low stability and bioavailability of Soy1 and Lup1, and hempseed protein hydrolysates.[17, 18] RADA16 is one of the well-studied ionic-complementary self-assembling peptides, characterized by an specific residue charge distribution pattern: + − + − with four cycles.[19] RADA16 can be synthesized using natural L-amino acids by solid-phase chemistry, which show inverted CD spectra in stable β-sheet in physiological solution or salt solution.[20] β-sheets can stack into a basic fiber unit and assembling into nanofibrils, consequently form ordered nanostructures as hydrogel with very high-water content (~99%). (Ref-Sun) Recently, many self-assembling peptides including RADA16 have been used in the delivery and functional enhancement of active oligopeptides because of there native extracellular matrix and favorable three-dimensional microenvironment.[21, 22] It has been reported that RADA16 has excellent biocompatibility and low immunogenicity, and its degradation products are amino acids, which do not cause tissue inflammation and do not affect the normal healing of tissues.[23] Nano-gelation

of the two active oligopeptides IPQVS and ELHQEEPL can bring many excellent properties such as biocompatibility, stability, and non-toxicity.[24]

In this research, the objective was to develop innovative nanogels that loaded the RAP1 and RAP2 into RADA16 scaffold. The linker of double Gly was used in the connection of RADA16 and the functional oligopeptide region (RAP1 and RAP2). The nano-gelation strategy given by RADA16 was studied in detail in this paper, including preparation condition, structural characterization and rheological determination. Whether the activity of the nano-gelled DPP-IV inhibitory peptides (RAP1 and RAP2) can be enhanced in the Caco-2 cell monolayer was the primary part we needed to explore. Additionally, the microstructure and the rheological behavior of RADA16-RAP1 and RADA16-RAP2 were characterized. Furthermore, their probable enhancement to stimulate GLP-1 secretion through activation of CaSR receptor was pursued in STC-1 cells.

2. Experimental

2.1 Materials

Dipeptidyl peptidase IV (DPP-IV from human, EC 3.4.14.5, ≥10 units per mg protein), Thioflavine T (C.I.No.49005), and Gly−Pro−p-nitroanilide were purchased from the Sigma-Aldrich Co. (St. Louis, Missouri, USA). Dulbecco's Modified Eagle Medium (DMEM), RPMI 1640, fetal bovine serum (FBS), Hank’s balanced salt solution (HBSS), and trypsin 0.025% with ethylenediaminetetraacetic acid disodium salt (EDTA) were all purchased from Gibco (Gaithersburg, MD, USA). A primary

antibody against human DPP-IV (ab 28340) and anti-CASR antibody (ab 19347) were obtained from Thermo Fisher Scientific (Waltham, MD, USA). RADA16 (Ac-RADARADARADARADA-NH_2), RAP1 (Ac-IPQVS-NH_2), RAP2 (Ac-ELHQEEPL-NH_2), RADA16-GG-RAP1, and RADA16-GG-RAP2 were synthesized via a solid-phase method using FMOC synthesis from LifeTein (New Jersey, USA) at >95% purity.

2.2 Preparation of Peptide Nanogels

The method used was based on the one by Pugliese *et al*.[17] with slight modifications. Ten mg of RADA16-GG-IPQVS, and RADA16-GG-ELHQEEPL were dissolved in 5 mL PBS (1×) solution or DMEM at room temperature, followed by ultrasonic bath for 20 min. This mixture was kept at 4°C overnight, resulting in the formation of the peptide nanogels. After the inversion experiment, different concentrations of nanogel peptides (from 10^{-6} M to 10^{-3} M) were prepared using the same method.

2.3 Rheological Analysis

The rheological properties of peptide nanogels were measured on a rheometer (DHR-2, TA, Instruments, New Castle, DE). The frequency sweep experiment was performed using a 1% (w/w, dilute 100 times) hydrogel. The storage modulus (G′) and loss modulus (G″) of the material were detected keeping strain rate (change of a deformation) at 1.0% with a continuous frequency (0.1−100 Hz). To examine the thixotropic property of peptide nanogels, 1% (w/w) peptide nanogel was used at a constant frequency of 1 Hz. The peptide nanogels were first measured under low constant strain of 0.1% for the initial 107 s, followed with a higher strain of 50% to

133 destroy the gel matrix. Subsequently, the strain was adjusted to a constant low level of
134 0.1%, and the restoration process was recorded.

135 **2.4 Circular Dichroism (CD), Atomic Force Microscopy (AFM) Image, and**
136 **Thioflavin T (ThT)-binding assay**

137 CD spectra were collected using a JASCO J-815 CD spectrometer (JASCO, Easton,
138 MD, USA). Peptide samples were prepared by diluting 1% peptides in water to a
139 working concentration of 25 μM. Samples were analyzed at room temperature in a
140 quartz cuvette with a path length of 0.5 cm and in a wavelength range 195–250 nm
141 and the Far-CD spectra were collected.

142 AFM was used to detect the morphology and structure of the RADA16-RAP1 and
143 RADA16-RAP2 nanogels. An aliquot of 1 μL peptide solution (100 μM) was placed
144 on a freshly cleaved mica sheet and observed with AFM (SPI4000 Probe Station and
145 SPA-400 SPM Unit, Seiko Instruments Inc, Chiba, Japan). Silicon tips (Si-DF20,
146 Olympus Corp, Tokyo, Japan) with a cantilever length of 200 μm and a spring
147 constant of 12 N/m were used. Typical scan parameters were as follows: Amplitude:
148 ~1 V, integral gain: ~0.25 V, proportional gain: ~0.03 V, and scan speed: 0.83–1 Hz.
149 The topographic images were recorded with 512 × 512 pixel resolution, in which the
150 brightness of morphology increased with height.

151 The method used was based on the one by Ghosh *et al*.[25] A stock solution of ThT of
152 5.0 mM concentration in PBS buffer (pH=7.4) was prepared which was then diluted
153 to 1.0 mM and filtered with a syringe filter. 50 μL of ThT solution was added to 1.95
154 mL of 0.5 mM peptide samples solution to make the final volume of 2.00 mL, and

after vortexing the mixture it was kept in the dark for about 2 h for efficient binding. Then the fluorescence spectrum was measured with excitation at 440 nm and recorded between 460 and 700 nm with 4 nm slits using a SpectraMax M2e Microplate Reader (Molecular Devices Inc., San Francisco, CA).

2.5 Cell Culture

Caco-2 cells (ATCC® HTB-37™) were purchased from American Type Culture Collection and grown in a T75 flask in DMEM containing 10% FBS, penicillin (100 U/mL), and streptomycin (100 μg/mL). STC-1 cells (ATCC® CRL-3254™) were purchased from American Type Culture Collection and grown in a T75 flask in RPMI 1640 containing 10% FBS, penicillin (100 U/mL), and streptomycin (100 μg/mL). Both cell lines were incubated at 37 °C in an atmosphere of 5% CO_2 and 90% relative humidity, and split at 80% to 90% confluency using 0.25% trypsin and 0.02% EDTA solution, respectively. The cells from passage numbers of 10 to 25 were used.

2.6 MTS assay for Cell Viability

In brief, Caco-2 cells or STC-1 cells suspension (100 μL) was incubated at a cell concentration of 4×10^4 cells/well in 96-well flat-bottomed plates. The cells were washed using PBS after incubation for 24 h at 37 °C. The samples solutions (100 μL) were added into the cell suspensions, which were cultured at 37 °C for another 24 h. After incubation, an aliquot of MTS solution (20 μL) was pipetted to each well, and the cells were cultured for 4 h. Finally, the absorbance of each well was read at 490 nm with a microplate reader (Power wave XS, Bio-TEK, USA). The results were expressed as the percent of viable cells compared with the control (% cell viability).

2.7 DPP-IV Inhibitory Effects in Caco-2 cell Monolayers

The DPP-IV inhibitory activity of peptide samples in Caco-2 cell monolayers were determined by the method of Lammi *et al*.[26] with slight changes. Caco-2 cells were seeded on black 96-well Transwell plates with clear bottoms at a density of 5×10^4 cells/well. The medium was regularly changed every other day. DPP-IV activity in Caco-2 cell monolayers was assayed on the 21 days after seeding. The cells were washed twice with 100 μL of PBS, and then spent media was discarded and the cells were treated with or without 100 μL of peptide sample (from 10^{-6} to 10^{-3} M) in growth DMEM medium for 60, 90, 180, and 360 min at 37 °C in an incubator with 5% CO_2. After washing the cells twice, 100 μL of Gly−Pro−p-nitroanilide substrate at the concentration of 50 μM in PBS was added to each well of black 96-well plates. Linear regressions % DPP-IV activity inhibition as a function of Ln (sample peptides): $y = 20.1x + 141.75$, $R^2 = 0.984$. Fluorescence signals (ex./em. 350/450 nm) were recorded using a microplate reader (Power wave XS, Bio-TEK, USA).

2.8 GLP-1 Secretion Effects in STC-1 Cells

GLP-1 release in STC-1 cells was performed using the method developed by Yang *et al*.[14] with some changes. STC-1 cells were seeded in 48-well plates (1.0×10^5 cells per well). After approximately 2 days of culture fusion, cell supernatants were removed and cells were washed twice with PBS, and the medium was replaced with three concentrations of peptide samples (50, 100, and 250 μM) in HEPES [4-(2-hydroxyethyl)-1-piperazineethanesulfonic acid] buffer, or HEPES buffer alone (negative control). Active GLP-1 was determined using a Glucagon Like Pepide-1

(Active) ELISA kit (EGLP-35 K, Millipore, Linco Research, Billerica, MA, USA) according to the manufacturer's instructions. The range of this assay was 1–333 pM. The inter-assay CV was 11% and the intra-assay CV was 6%. When necessary, samples were diluted in assay buffer from the kit to be within the detection range of this assay.

2.9 Immunofluorescence and Laser-Scanning Microscopy

After treatment without peptide samples or with 250 μM RAP1, RAP2, RADA16-RAP1, and RADA16-RAP2, respectively, the Caco-2 cell monolayers or STC-1 cells were washed twice with PBS, and then fixed with a 4% paraformaldehyde aqueous solution for 10 min, and then permeabilized with 0.2% Triton X-100 for 5 min at 20 °C. After blocking with 5% bovine serum albumin (BSA) in PBS for 1 h at 20 °C, the cells were incubated with primary antibodies (1:50, diluted in 5% BSA) overnight at 4 °C. Next, the biotinylated secondary antibody was applied for 90 min with 4′,6-diamidino-2-phenylindole counterstaining. The images were acquired using a fluorescence microscope LSM 700 confocal laser scanning microscope (Zeiss Co. Ltd, Germany).

2.10 Western-Blotting (CaSR)

After the treatment of peptide samples or no treatment, the supernatant and STC-1 cell lysates were collected. The protein concentrations were determined using Lowry assay. Aliquots of protein (10 μg) were separated by 12% sodium dodecyl sulfate–polyacrylamide gel electrophoresis (SDS–PAGE) and were transferred onto polyvinylidene difluoride membranes (Millipore, MA, USA). The membranes were

221 blocked with 5% nonfat dry milk/ 0.1% Tween 20/TBS for 2 h and then were
222 incubated with the primary antibody CaSR with gentle shaking for 8–12 h overnight
223 at 4 °C, followed by incubation with horseradish peroxidase (HRP)-conjugated
224 secondary antibodies for 2 h at room temperature. The blots were then exposed, and
225 chemiluminescent images were captured by a Bio-Rad Chemi Doc XRS machine. A
226 GAPDH antibody was used as an internal control to show the equality of protein
227 levels loaded.

228 **2.11 Determination of Intracellular Calcium Ion Mobilization and cAMP**
229 **Concentration**

230 Intracellular calcium ion mobilization and cAMP concentration were determined by
231 the method of Zhou *et al*.[27] and Kondrashina *et al*.[28] with slight changes. STC-1 cells
232 were grown on glass coverslips in 6-well plate at density of 1×10^5 cells/well. After
233 the cells reached 80%-90% confluence, the slides were washed with HBSS and then
234 stained with 5 μM Fluo-4 AM in bath solution consisting of HBSS supplemented with
235 20 mM of HEPES buffer. A 100 μL of peptide samples or HEPES were added to the
236 glass slide. LSM 700 confocal laser scanning microscope (Zeiss Co. Ltd, Germany)
237 was used to measure the intracellular calcium ion mobilization in the STC-1 cells.
238 Fluo4 fluorescent was recorded every 6.0 s at an excitation wavelength of 488 nm and
239 calculated the changes by: $\Delta F/F = (F-F_0)/F_0$. After cell exposure to control or peptide
240 samples, the supernatant was removed, and the cells were lysed with 0.2 mL of 0.1 M
241 HCl for 10 min at room temperature. Following centrifugation at 1000× g at 4 ˚C for
242 5 min, cAMP level in the supernatants was assayed by cAMP ELISA kit according to

the manufacturers' instructions.

2.12 Statistical Analysis

All data performed in triplicate are expressed as means ± SEM. Statistical analysis was performed by paired samples t-test or one-way analysis of variance (ANOVA) in GraphPad prism 6.0 (GraphPad Software Inc., La Jolla, CA, USA). P values less than 0.05 were considered statistically significant.

3. Results and discussion

3.1 Preparation and Characterization of RADA16-RAP1 and RADA16-RAP2 nanogels

RADA16-RAP1 and RADA-RAP2 formed nanogels under mild conditions, which contributed to the scaffold of -Gly Gly-. As shown in **Fig. 1A**, RADA16-RAP1 and RADA16-RAP2 not only self-assembled in PBS to form nanogels, but also in DMEM. Interestingly, as shown in **Fig. 1B**, RADA16-RAP1 gelated at a concentration of 2 mg/mL at pH 6.5; as shown in **Fig. 1D** while no nanogel was produced in the alkaline environment (pH=8.5). The main features were high stability and dispersibility in water, and low temperature; 37 °C hardly destroyed its spatial structure. Differently, Lammi *et al.* developed a method to retain DPP-IV inhibitory peptides[21] and hydrolysates[22] in the structure of RADA16 gel fiber, which was just a physical cross between nanofibrous structures and did not involve chemical bonding. Of course, this peptide-bonded oligopeptide sequence has also been reported, which can self-assemble in a wild environment to form a nanoscale hydrogel. For example, two

amino acids (-Gly Gly-) were placed between RADA16 and both neurotrophic CTDIKGKCTGACDGKQC and RGIDKRHWNSQ, the structure of which promoted the neurite outgrowth of PC12 cells significantly compared to non-functionalized peptide;[29] polyethylene glycol (PEG) was used to enhanced the transportation efficiency and stability of a designed basic oligopeptide (CHHRHRHHC).[30] Functionalized self-assembling peptides based on RADA16 using novel scaffolds such as -Gly Gly- or PEG were stable than physical mixture.[31] Therefore, the nanogel in this study was based on the molecular unit of RADA16-GG-Xaa, which might have advantages of better-controlled preparation of the final product and exposed functional peptides fragment on both sides of the nanofiber.

AFM images in **Fig. 2A-E** revealed that both studied peptides, RADA16-RAP1 and RADA16-RAP2 formed nanofibers in the aqueous environment. According to the Fig. 2F, the width (approximately 1-10nm) and length (approximately 50-1000 nm) of the fibrous structure of RADA16-RAP1 and RADA-RAP2 can be qualitatively. As depicted in **Fig. 2G**, we observed a negative band at 216 nm and a positive band at 195 nm in the CD spectra of RADA16, RADA16-RAP1, and RADA16-RAP2. CD spectra studies showed that RADA16-RAP1 and RADA16-RAP2 had a high propensity to self-assemble into very stable β-sheet structures. As shown in **Fig. 2H**, there is a fluorescence intensity peaked at 500 nm closed to the sample with only RADA16, the formation of β-sheet amyloid type fibril was further confirmed by ThT binding assay. The sequence and nature of amino acid residues directly determine the spatial structure of the formed peptide nanogels. For example, Silva *et al*.[32] reported a

great potential of LLKKK18-loaded nanogels using for tuberculosis therapeutics; Min *et al*.[33] reported a covalently self-assembled peptide nanogel from a tyrosine-rich peptide monomer; Shimoda *et al*.[34] reported a cell specific peptide (Ac-RGD-NH_2)-modified nanogel using for its potential to act as a protein delivery carrier. The sequence RADARADARADARADA in the prepared peptide nanogel is a cyclic sequence of alternating hydrophobic and hydrophilic amino acid, which determines the amphiphilicity of the polypeptide.[35, 36] Amino acids with different charges contained on the hydrophilic surface drive each polypeptide to aggregate to form a β-sheet structure through electrostatic interaction, and further form a nanofibrous structure.[37, 38] Cormier *et al*.[15] reported that the thickness of the nanofibers proved to be composed of two stacked β-pleated sheets using NMR analysis.

3.2 Injectability and Shear-Thinning Propensity of RADA16-RAP1 and RADA16-RAP2

In an attempt to elucidate the injectability and shear-thinning propensity of RADA16-RAP1 and RADA16-RAP2, rheological properties of these features were studied in detail. As shown in **Fig. 4A** and **B**, with the strain constant from 0.1%-1.0%, both the storage modulus (G′) and loss modulus (G″) of the two peptide nanogels were stationary. Thus, we chose strain=1.0% as the parameter for the next frequency experiment. Compared to RADA16-RAP2, RADA16-RAP1 was more likely to become a fluid under strain because the value of the abscissa corresponding to the intersection was lower. The intersection point of G' and G'' represents the

309 critical point of the nanogel transition from solid phase to liquid phase, which can be
310 named yield strain. **Fig. 4C** and **D** show that G′ values of the two peptide nanogels
311 were generally one order of magnitude greater than the G″, which showed the typical
312 soft hydrogel profiles. In addition, both the G′ and G″ of the two-peptide nanogels
313 were slightly dependent on the frequency (0.1−100 Hz) when keeping strain constant
314 at 1.0%, indicating a formation of a stable nanogel. The G' and G'' of
315 RADA16-RAP2 was slightly lower than that of RADA16-RAP1, which may be
316 related to the hydrophobicity of functional peptides. Furthermore, the two peptide
317 nanogels were first tested under low constant strain of 0.1% for the first 107 s,
318 followed with a higher strain of 50% to rupture the gel matrix. The strain was adjusted
319 to the previous constant low level of 0.1%, and the restoration process were recorded.
320 It can be seen that both of the two-peptide nanogels could gradually recover most of
321 their original strength at 158 s after the withdrawal of the large strain, suggesting a
322 good rheological nature for injectable applications (**Fig. 4E** and **F**). The injectability
323 and good rheology of RADA16-RAP1 and RADA16-RAP2 indicated that they not
324 only can be taken orally, but subcutaneous tissue injection is also an alternative
325 solution. Although our research is the first attempt to prepare nanogels by
326 -Gly-Gly-covalently linking RADA16 and DPP-IV inhibitory peptides, this
327 technology has been widely used in the medical field. Recently, RADA16-assisted
328 molecular designed method was applied to DPP-IV and ACE inhibitory peptides
329 IAVPTGVA and LTFPGSAED. Similarly, RADA16-IAVPTGVA and RADA16-
330 LTFPGSAED had the typical profile of soft hydrogels alike RADA16-RAP1 and

RADA16-RAP2.[21] In clinical aspect, a variety of peptide nanogels that promote tissue regeneration are self-assembled by ion-complementary peptides such as RADA16.[37, 39-41] In order that RADA16-RAP1 and RADA16-RAP2 can be injected subcutaneously, the study of thixotropy is of great significance. As we known, DPP-IV has a widespread organ distribution, and its expression level differs greatly between tissues.[42] As an alternative injectable drug, RADA16-RAP1 and RAP2 can act more efficiently on DPP-IV in the body. Jin *et al*.[16] found that the nanogel peptides in plasma could effectively protect the functional peptides fragment, thereby enhancing their bioavailability. It is well known that insulin is poorly oral and GLP-1 agonist is poorly injected.[43, 44] For the development of hypoglycemic drugs, both oral and injection characteristics will bring good news to the majority of type 2 diabetes patients. Therefore, injectable RADA16-RAP1 and RADA16-RAP2 are expected to provide a treatment targeting DPP-IV for diabetic patients with absorption disorders.

3.3 Viability of Caco-2 Cells and STC-1 Cells Exposure to Different Concentrations of Peptide Samples.

In this study, MTS assay was used to detect the cytotoxicity of the original peptides and the nanogel peptides. Compared to the MTT assay, the MTS assay is highly water-soluble, faster to use, and more specific.[45] As illustrated in **Fig. 3A-D**, the effect of RAP1, RADA16-RAP1, RAP2 and RADA16-RAP2 on Caco-2 cell viability is observed, respectively. With the concentration of each of the peptide samples increasing, the viability of the Caco-2 cells decreased slightly, which was more than 95%. In contrast, there was no effect of peptide samples treatment on the STC-1 cells

(**Fig. 3E-H**). It can be concluded that each of peptide samples had no significant cytotoxicity in the two types of cell models at the concentrations from 0 to 1.0 mM. For subsequent experiments the doses lower than 1.0 mM were used to examine the effect of the oligopeptides and peptide nanogels.

3.4 RADA16-RAP1 and RADA16-RAP2 Enhance the DPP-IV inhibitory Activity

As shown in **Table 1**, RADA16-RAP1 and RADA16-RAP2 gave lower values (decreased by 26.4% and 17.5%) of DPP-IV inhibition IC_{50} in Caco-2 cell monolayers compared to RAP1 and RAP2, respectively. As illustrated in **Fig. 5A** and **B**, the decrease in the fluorescence signals corresponding to DPP-IV activity was reduced by over 24.61% and 21.42% in the presence of 250 μM RADA16-RAP1 and RADA16-RAP2 respectively, compared with the control (p<0.01). Also, the assistance of RADA16 reduced the fluorescence intensity of DPP-IV by 10% compared with the original oligopeptides (RAP1 and RAP2). **Fig. 6A** and **B** highlighted that RADA16-RAP1 dropped the DPP-IV activity by 53.88%, 64.20%, 66.85%, and 69.28% after 60, 90, 180, and 360 min, respectively; whereas RADA-RAP2 dropped by 52.70%, 54.98%, 58.07%, and 64.68%, respectively, which were all lower activities than the original oligopeptides at different time periods. It has been reported that gelation of oligopeptides could play an important role in disease treatment and surgical recovery, due to its biocompatibility.[31, 46] Thus, we infer that DPP-IV inhibitory peptides IPQVS and ELHQEEPL can form a nanogel with high water content close to human cells and tissues through the self-assembly gelation of RADA16. They can be attached more firmly to the brush border of human small

intestinal epithelial cells to inhibit the effect of the DPP-IV enzyme in the intestinal lumen. As our previously reported,[7] peptide nanogels with RAP1 and RAP2 functional structures could not change the expression of DPP-IV gene, but decrease the activity of DPP-IV. In addition to degradation during gastrointestinal digestion, the original structure of most of the oligopeptide can also be altered and modified on the intestinal epithelial cells.[47] The Caco-2 cells used in this study were differentiated and cultured on Transwell plates for 21 days, which can simulate the function of intestinal epithelial cells. The improvement of DPP-IV inhibitory activity indicated that the nano-gelation successfully prevented the structural destroyed of RAP1 and RAP2 by enteropeptidase in the intestinal epithelial cells.

3.5 RADA16-RAP2 and Hydrolyzed RADA16-RAP1 Enhance the Capacity of Enabling the GLP-1 Secretion via CaSR pathway

As shown in **Table 2**, the 60 min exposure of STC-1 cells to 50-250 μM RAP2 and RADA16-RAP2 led to the release of GLP-1 in a dose–response manner. At the condition of treatment with thermolysin, the ability of RAP1 to stimulate GLP-1 secretion was improved, which the content of GLP-1 in STC-1 cells significantly increased (p<0.05) from 10.04 pM to 32.63 pM at concentration of 250 μM. Conversely, the addition of thermolysin reduced the amount of the GLP-1 stimulated by RAP2 in STC-1 cells, which approximately caused an average drop of 41.62% decline at three concentrations (50 μM, 100 μM, 250 μM). Thermophilic protease is a thermally stable metalloproteinase, which can preferentially enucleate the N-terminal of hydrophobic amino acid residues, including leucine (Ile) and valine (Val).[48]

Therefore, it can be speculated that the effective hydrolytic fragments in RAP1 are IPQ, PQ, and Q, the same report is Reimann *et al.*[49] found that glutamine or small peptides with glutamine residues at both ends of the peptide chain can significantly increase GLP-1 secretion of endocrine cells in the small intestine. The addition of the DPP-IV had no negative effect ($p>0.05$) on the GLP-1 release stimulated by RADA16-RAP2, but not RAP2, RAP1, and RADA16-RAP1. This phenomenon indicated that the nanogel structure of RADA16 can promote RAP2 to resist the hydrolysis of DPP-IV. It was also proved from another perspective that the DPP-IV inhibition types of RAP1 and RAP2 reported in the previous study were correct.[2] In brief, the RADA16-RAP2 based hydrogel structure could better avoid the weakening of the GLP-1 stimulated effect when thermolysin and DPP-IV participated. As shown in **Fig. 7A**, exposure of STC-1 cells to 150 μM and 250 μM RAP2 led to an increased ($p<0.05$) CaSR expression in protein level after 60 min of perfusion, compared to that of the control group without RAP2. Whereas, no significant changes were observed in the TGR5 (G protein-coupled bile acid receptor) protein expression ($p>0.05$). In agreement with our previous observations in the DPP-IV inhibitory effect, RADA16-based nanogel RADA16-RAP2 could enlarge the CaSR activation versus RAP2 at the concentration of 250 μM (**Fig. 7B**). **Fig. 7C** intuitively reflected the activation of CaSR in STC-1 cells stimulated by RAP2 and RADA16-RAP2, which the red fluorescence represented CaSR. According to **Fig. 7C**(d), the increase (approximate fourteen-folds than RADA16) of the relative value of red fluorescence indicated that the expression of CaSR was significantly ($p<0.01$) increased by

RADA16-RAP2 in STC-1 cells. Although the red fluorescence of RAP2 group was also increased (approximate eight-folds than RADA16), but not as significant as that of RADA16-RAP2 group. RADA16 itself had no activity to stimulate CaSR expression, and it is the Gly-Gly linked functional peptide fragment RAP2 that gave function to its peptide chain skeleton. In order to study the downstream of CaSR after being activated by the RAP2 and RADA16-RAP2, the inherent content of Ca^{2+} in STC-1 cells was assessed. In **Fig. 8A**, the confocal microscopy studies revealed that the exposure to 250 μM RAP2 and RADA16-RAP2 caused increased $[Ca^{2+}]_i$ mobilization in STC-1 cells, compared to the control ($p<0.05$). However, the content of cAMP in STC-1 cells stimulated by RAP2 and RADA16-RAP2 was both approximately equal to 1.5-fold ($p<0.05$) than that of the control (**Fig. 8B**). The above experiments proved that RADA16-RAP2 and hydrolyzed RADA16-RAP1 enhanced the capacity of enabling the GLP-1 secretion via CaSR pathway.

The strategy of gelation based on RADA16 weakened the degradation and activity reduction of DPP-IV inhibitory peptide in intestinal epithelial cells, in addition, the agonistic effect of RAP2 on CaSR has also been enhanced. It has been reported that oligopeptides stimulate GLP-1 secretion through two pathways, including PEPT1-dependent electrogenic uptake and activation of CaSR.[50] It has been reported that oligopeptides containing aromatic amino acids can regulate the secretion of GLP-1, PYY and other hormones by mediating CaSR on the surface of intestinal epithelial cells.[51] For the CaSR pathway, the related receptor GPRC6A underlie γ-[Glu](n=1,2)-Phe/-Met/-Val-stimulated GLP-1 secretion from STC-1 cells; and

441 ornithine-stimulated GLP-1 secretion from GLUTag cells.[14, 52] The VFT domain is the
442 docking site for the interaction between oligopeptides and CaSR.[53, 54] Moreover, the
443 kokumi-flavor peptides can be positively correlated with the activation of CaSR,[55]
444 whether the peptide we found has kokumi-flavor remains to be verified. However, due
445 to the interconversion flux of cATP and cAMP in the STC-1 cell is limited,[56] the
446 effects of RAP2 and RADA16-RAP2 at the concentration of 250 μM on the cAMP
447 content in STC-1 were almost equal. Similar to the results in this section, the blue
448 whiting (*Micromesistius poutassou*) protein hydrolysate (2.5 mg/mL) reported by
449 Harnedy *et al*.[57] could increase the levels of calcium and cAMP in pancreatic
450 BRIN-BD11 cells, suggesting that the mechanism by which oligopeptides promote
451 GLP-1 secretion by regulating level of intracellular calcium ion is widely found in
452 different cells of the body.
453
454 **Conclusions**
455 In addition to processing and environmental conditions affecting the DPP-IV
456 inhibitory activity by peptides or hydrolysates,[58, 59] poor stability and low
457 bioavailability are the main constraints for the development of peptides. In an attempt
458 to overcome these problems, the innovated and harmless nanogel with the sequence of
459 RADA16-RAP1 and RADA16-RAP2 were developed to be used for enhancing the
460 DPP-IV inhibitory activity. Meanwhile, the fortified activation effect by
461 RADA16-RAP2 on GLP-1 secretion in STC-1 cells was found. In future work, (1)
462 animal experiments will be applied to the activity evaluation and injection effect of

rapeseed napin derived nanogel peptides; (2) The linkage of functional peptides RAP1 and RAP2 at the opposite terminal of RADA16 will be studied, and the differences between the new linkage and the one reported in this paper will be compared. The results offer great promise in applications such as absorbable macromolecular hypoglycemic drugs.

Author contributions:

F.X. designed the research, collected and analyzed the data, composed the manuscript. B.X. designed parts of the research, provided parts of experimental instruments. H.C. collected and analyzed data, revised and edited the manuscript. E.dM. designed parts of the research, revised and edited the manuscript. X.J. designed the research, edited the manuscript.

Notes

The authors declare no competing financial interest.

Acknowledgments

This work was supported by the USDA-HATCH; the Fundamental Research Funds for the Central Universities (China)

Abbreviations used

AFM, Atomic Force Microscopy; **cAMP,** cyclic adenosine monophosphate; **CaSR,**

485 Calcium-sensing Receptor; **CD,** Circular dichroism; **DPP-IV,** Dipeptidyl
486 peptidase-IV; **G',** Storage modulus; **G'',** Low modulus; **GLP-1,** Glucagon-like
487 peptide 1; **MTS,**
488 3-(4,5-dimethylthiazol-2-yl)-5-(3-carboxymethoxyphenyl)-2-(4-sulfophenyl)-2H-tetra
489 zolium; **PEG,** Polyethylene glycol; **RAP1,** Ac-IPQVS-NH_2; **RAP2,**
490 Ac-ELHQEEPL-NH_2; **RADA16,** Ac-RADARADARADARADA-NH_2.
491

492 **References**

493 1. H. John, E. Maronde, W. Forssmann, M. Meyer and K. Adermann. *Eur. J. Med.*
494 *Res.*, 2008, **13**(2), 73.
495 2. F. Xu, Y. Yao, X. Xu, M. Wang, M. Pan, S. Ji, J. Wu, D. Jiang, X. Ju and L.
496 Wang. *J. Agric. Food Chem.*, 2019, **67**(13), 3679-3690.
497 3. E. Seki, E.; A. Yamamoto, Y. Fujiwara, T. Yamane, H. Satsu and I. Ohkubo. *J.*
498 *Agric. Food Chem.* 2020, **68**(23), 6355-6367.
499 4. T. Mochida, T. Hira and H. Hara. *Endocrinology*, 2010, **151**(7), 3095 —3104.
500 5. Y. Ishikawa, T. Hira, D. Inoue, Y. Harada, H. Hashimoto, M. Fujii, M. Kadowaki
501 and H. Hara. *Food Funct.*, 2015, **6**(8),2525-2534.
502 6. F. O'Halloran, C. Bruen, B. McGrath, H. Schellekens, B. Murray, J.F. Cryan, A.L.
503 Kelly, P. L. H. McSweeney and L. Giblin. *Food Chem.*, 2018, **252**, 303-310.
504 7. F. Xu, E. G. de Mejia, H. Chen, K. Rebecca, M. Pan, R. He, Y. Yao, L. Wang and
505 X. Ju. *J. Food Biochem*., 2020, **44**(10), e13406.
506 8. T. Ohsu, Y. Amino, H. Nagasaki, T. Yamanaka, S. Takeshita, T. Hatanaka, Y.

Maruyama, N. Miyamura and Y. Eto. *J. Biol. Chem.* 2010, **285**(2), 1016– 1022.

9. S. Nakajima, T. Hira, Y. Eto, K. Asano and H. Hara. *Regul. Pept*. 2010, **159**(1-3), 148– 155.

10. L. Gama, L. M. Baxendale-Cox and G. E. Breitwieser. *Am. J. Physiol*. 1997, **273**(4), C1168– C1175.

11. S. Guo, T. Yan, L. Shi, A. Liu, T. Zhang, Y. Xu, W. Jiang, Q. Yang, L. Yang, L. Liu, R. Zhao, and S. Zhang. *Phytomedicine*. 2021, **84**, 153507.

12. D. A. Goldspink, V. B. Lu, E. L. Miedzybrodzka, C.A. Smith, R. E. Foreman, L. J. Billing, R. G. Kay, F. Reimann and F. M. Gribble. *Cell. Rep.*, 2020, **31**(13), 107833.

13. J. Ohki, A. Sakashita, E. Aihara, A. Inaba, H. Uchiyama, M. Matsumoto, Y. Ninomiya, T. Yamane, Y. Oishi and K. Iwatsuki. *Biosci. Biotechnol. Biochem*., 2020, **84**(5), 936-942.

14. J. Yang, W. Bai, X. Zeng and C. Cui. *Food Funct.*,2019, **10**(7), 4071-4080.

15. A. R. Cormier, X. Pang, M. I. Zimmerman, H. X. Zhou and A. K. Paravastu. *ACS nano*, 2013, **7**(9), 7562-7572.

16. H. Jin, C. Wan, Z. Zou, G. Zhao, L. Zhang, Y. Geng, T. Chen, A. Huang, F. Jiang, J. P. Peng, J. F. Lovell, J. Chen, G. Wu and K. Yang. *Acs Nano*, 2018, **12**(4), 3295-3310.

17. R. Pugliese, C. Bollati, F. Gelain, A. Arnoldi and C. Lammi. *J. Agric. Food Chem.*, 2019, **67**(13), 3615-3623.

18. C. Lammi, C. Bollati, F. Gelain, A. Arnoldi and R. Pugliese. *Front. Chem*., 2019,

6, 670.

19. S. Sankar, K. O'Neill, M. Bagot D'Arc, F. Rebeca, M. Buffier, E. Aleksi, M. Fan, N. Matsuda, E. Seok Gil, and L. Spirio. *Front. Bioeng. Biotechnol.*, 2021, 9, 465.
20. F. Gelain, Z. Luo, and S. Zhang. *Chem. Rev.*, 2020, 120(24), 13434-13460.
21. R. Pugliese, M. Bartolomei, C. Bollati, G. Boschin, A. Arnoldi, and C. Lammi, *Biomedicines*, 2022, 10(2), 330.
22. S. Koutsopoulos. *J. Biomed. Mater. Res. Part A*, 2016, **104**(4) 1002-1016.
23. R. Wang, Z. Wang, Y. Guo, H. Li, and Z. Chen. *J. Biomater. Sci.-Polym. Ed.*, 2019, **30**(9), 713-736.
24. L. Jiang, C. Liu, K. Mayumi, K. Kato, H. Yokoyama and K. Ito. *Chem. Mat.*, 2018, **30**(15), 5013-5019.
25. G. Ghosh, R. Barman, J. Sarkar, and S. Ghosh. *J. Phys. Chem. B*, 2019, 123(27), 5909-5915.
26. C. Lammi, C. Bollati, S. Ferruzza, G. Ranaldi, Y. Sambuy and A. Arnoldi. *Nutrients*, 2018, **10**(8), 1082.
27. H. R. Zhou and J. J. Pestka. *Toxicol. Sci.*, 2015, **145**(2), 407-417.
28. A. Kondrashina, D. Papkovsky and L. Giblin. *Mol. Nutr. Food Res.*, 2018, **62**(3), 1700568.
29. C. Lu, Y. Wang, S. Yang, C. Wang, X. Sun, J. Liu, H. Ying, W. Jiang, H. Meng, F. Rao, X. Wang and J. Peng. *ACS Biomater. Sci. Eng.*, 2018, **4**(8), 2994-3005.
30. T. Kanazawa, M. Kaneko, T. Niide. F. Akiyama, S. Kakizaki, H. Ibaraki, S. Shiraishi, Y. Takashima, T. Suzuki and Y. Seta. *Int. J. Pharm.*, 2017, **530**(1-2):

195-200.

31. E. Busseron, Y. Ruff, E. Moulin and N. Giuseppone. *Nanoscale*, 2013, **5**(16): 7098-7140.
32. J. P. Silva, C. Gonçalves, C. Costa, J. Sousa, R. Silva-Gomes, A. G. Castro, J. Pedrosa, R. Appelberg and F. M. Gama. *J. Control. Release*, 2016, **235**, 112-124.
33. K. I. Min, D. H. Kim,H. J. Lee, L. Lin and D. P. Kim. *Angew. Chem.-Int. Edit.*, 2018, **130**(20), 5732-5736.
34. A. Shimoda, S. L. Sawada and K. Akiyoshi. *Macromol. Biosci.*, 2011, **11**(7), 882-888.
35. L. M. D. L. Rodriguez, Y. Hemar, J. Cornish and M. A. Brimble. *Chem. Soc. Rev.*, 2016, **45**(17), 4797-4824.
36. H. Tao, Y. Wu, H. Li, C. Wang, Y. Zhang, C. Li, T. Wen, X. Wang, Q. He, D. Wang and D. Ruan. *ACS Appl. Mater. Interfaces*, 2015, **7**(31), 17076-17087.
37. T. Y. Cheng, H. C. Wu, M. Y. Huang, W. H. Chang, C. H. Lee and T. W. Wang. *Nanoscale*, 2013, **5**(7), 2734-2744.
38. T. Vermonden, R. Censi and W. E. Hennink. *Chem. Rev.*, 2012, **112**(5), 2853-2888.
39. Y. Sun, W. Li, X. Wu, N. Zhang, Y. Zhang, S. Ouyang, X. Song, X. Fang, R. Seeram, W. Xue, L. He and W. Wu. *ACS Appl. Mater. Interfaces*, 2016, **8**(3), 2348-2359.
40. A. R. Cormier, C. Ruiz-Orta, R. G. Alamo and A. K. Paravastu. *Biomacromolecules*, 2012, **13**(6), 1794-1804.

41. H. Jin, G. Zhao, J. Hu, Q. Ren, K. Yang, C. Wan, A. Huang, P. Li, J. P. Feng, J. Chen and Z. Zou. *ACS Appl. Mater. Interfaces*, 2017, **9**(31), 25755-25766.

42. A. M. Lambeir, C. Durinx, S. Scharpé, and I. De Meester. *Crit. Rev. Clin. Lab. Sci.*, 2003, **40**(3), 209-294.

43. C. Y. Wong, H. Al-Salami, and C. R. Dass, *J. Control. Release*, 2017, **264**, 247-275.

44. N. G. Eissa, M. Elsabahy, and A. Allam. *Int. J. Pharm.*, 2021, 120317.

45. M. I. Patel, R. Tuckerman, Q. Dong. *Biotechnol. Lett.*, 2005, **27**(11), 805-808.

46. C. Liang, D. Zheng, F. Shi, T. Xu, C. Yang, J. Liu, L. Wang and Z. Yang. *Nanoscale*, 2017, **9**(33), 11987-11993.

47. C. Zhang, H. Liu, S. Chen, and Y. Luo. *Food Funct.*, **9**(4), 2240-2250.

48. G. Morgan, and J. S. Fruton. *Biochemistry*, 1978, **17**(17), 3562-3568.

49. F. Reimann, L. Williams, G. da Silva Xavier, G. A. Rutter, and F. M. Gribble. *Diabetologia*, 2004, **47**(9), 1592-1601.

50. E. Diakogiannaki, R. Pais, G. Tolhurst, H. E. Parker, J. Horscroft, B. Rauscher, T. Zietek, H. Daniel, F. M. Gribble and F. Reimann. *Diabetologia*, 2013, **56**(12), 2688-2696.

51. I. Acar, A. Cetinkaya, I. Lay, and E. Ileri-Gurel. *Nutr. Neurosci.*, 2020, **23**(6), 481-489.

52. M. Oya, T. Kitaguchi, R. Pais, F. Reimann, F. Gribble and T. Tsuboi. *J. Biol. Chem*., 2013, **288**(7), 4513-4521.

53. G. K. Broadhead, H. C. Mun, V. A. Avlani, O. Jourdon, W. B. Church, A.

595 Christopoulos, L. Delbridge and A. D. Conigrave. *J. Biol. Chem.*, 2011, **286**(11),
596 8786-8797.
597 54. D. Guo, H. He and T. Hou. *Food Chem*., 2020, **325**, 126919.
598 55. J. Yang, W. Bai, X. Zeng, and C. Cui. *Trends Food Sci. Technol.*, 2019, **91**,
599 339-346.
600 56. T. S. McQuaid, M. C. Saleh, J. W. Joseph, A. Gyulkhandanyan, J. E.
601 Manning-Fox, J. D. MacLellan, M. B. Wheeler and C. B. Chan. *J. Endocrinol.*,
602 2006, **190**(3), 669-680.
603 57. P. A. Harnedy, V. Parthsarathy, C. M. McLaughlin, M. B. O'Keeffe, P. J. Allsopp,
604 E. M. McSorley, F. P. M. O'Harte and R. J. FitzGerald. *J. Funct. Foods*, 2018. **40**,
605 137-145.
606 58. L. Mojica, K. Chen and E. G. de Mejía. *J. Food Sci.*, 2015, **80**(1), H188-H198.
607 59. I. M. Lacroix, X. M. Chen, D. D. Kitts and E. C. Li-Chan. *Food Funct.*, 2017, **8**(2),
608 701-709.
609
610
611
612
613
614
615
616

617

618

619

620 **Figure legends**

621 **Figure 1.** Photographs of peptide nanogels loaded with various agents. (A1). 1×PBS
622 without peptides; (A2). RADA16-GG-IPQVS in 1×PBS at pH 6.5 (adjusted with
623 HCl); (A3). RADA16-GG-ELHQEEPL in 1×PBS; (A4). DMEM without peptides;
624 (A5). RADA16-GG-IPQVS in DMEM at pH 6.5 (adjusted with HCl); (A6).
625 RADA16-GG-ELHQEEPL in DMEM; (B). RADA16-GG-IPQVS in 1×PBS at pH
626 6.5 (adjusted with HCl); (C). RADA16-GG-IPQVS in 1×PBS; (D).
627 RADA16-GG-IPQVS in 1×PBS at pH 8.5 (adjusted with $NaHCO_3$). (E). Schematic
628 diagram of preparation of RADA16-GG-IPQVS and RADA16-GG-ELHQEEPL.

629 **Figure 2.** Characterization of oligopeptides and peptide nanogels. (A). Atomic force
630 microscopy **(**AFM) image of RAP1; (B). AFM image of RAP2; (C). AFM image of
631 RADA16; (D). AFM image of RADA16-RAP1; (E). AFM image of RADA16-RAP2;
632 (F). Graphical representation of AFM; (G). Far-UV circular dichroism (CD) spectra
633 plotting the mean residue ellipticity (mdeg) against wavelength (nm) for RADA16,
634 RAP1, RAP2, RADA16-RAP1, and RADA16-RAP2. (H). Thioflavin T (ThT)
635 fluorescence assay of RADA16, RADA16-RAP1, and RADA16-RAP2.

636 **Figure 3**. Rheological property of oligopeptides and peptide nanogels. Rheological
637 strain oscillatory rheology of (A). RADA16-RAP1 in 1×PBS at pH 6.5 (adjusted with
638 HCl); (B). RADA16-RAP2 in 1×PBS. Frequency sweep rheological analysis; (C).

RADA16-RAP1 in 1×PBS at pH 6.5 (adjusted with HCl); (D). RADA16-RAP2 in 1×PBS. Thixotropic test of RADA16-RAP1 in 1×PBS at pH6.5 (adjusted with HCl) and RADA16-RAP2 in 1×PBS: (E) and (F). Step–strain measurement with applied oscillatory strain alternated between 0.1% for 107s periods and 50% for 50s periods (ω=1.0 Hz, 25°C). Sample was liquid when G''≥G'.

Figure 4. Cytotoxicity of RADA16, RAP1, RAP2, RADA16-RAP1, and RADA16-RAP2 in Caco-2 cell monolayers and STC-1 cells.

Figure 5. (A) and (B), Confocal laser scanning microscopy depicting two-dimensional fluorescence detection and quantification, determined by the intensity (AU) over area (μm^2) of DPP-IV in Caco-2 cell monolayers after 250 μM treatments with peptide samples, total DPP-IV intensity was normalized to DAPI staining. Different letters (a–c) represent significant differences at $p<0.05$.

Figure 6. Percent *in vitro* activity of DPP-IV expressed on Caco-2 cell monolayers after treatment with peptide samples (at concentration of 250 μM) at 60, 90, 180, and 360 min. (A). RAP1 and RADA16-RAP1. (B). RAP2 and RADA16-RAP2.

Figure 7. STC-1 cells express calcium-sensing receptor (CaSR). (A). Western-blotting of CaSR at different concentrations of RAP2. (B). Western-blotting of CaSR at 250 μM of RADA16, RAP2 and RADA16-RAP2. (C). Confocal laser scanning microscopy depicting two-dimensional fluorescence detection and quantification, determined by the intensity (AU) over area (μm^2) of CaSR in STC-1 cells: a. RADA16(250 μM); b. treatment with RAP2(250 μM); c. treatment with RADA16-RAP2(250 μM). *represents significant differences at $p<0.05$, **represents

661 significant differences at p<0.01.

662 **Figure 8.** (A). The intracellular Ca^{2+} mobilization. (B). determination of cAMP
663 content in STC-1 cells. *represents significant differences at p<0.05, **represents
664 significant differences at p<0.01.

Table 1 IC_{50}[a] changes of RAP1, RAP2, RADA16-RAP1, and RADA16-RAP2 following incubation with Caco-2 cell monolayers.

Group	Sequence	Mass (Da)	Retention time (min)[b]	DPP-IV-inhibition IC_{50} (μM) *	
				Chemical substrate-enzyme	In Caco-2 cell monolayers
1	RAP1	542.6209	10.322	52.16 ± 5.91 a	101.66 ± 6.02 c
2	RAP2	993.4767	12.315	78.46 ± 4.94 a	112.29 ± 5.27 c
3	RADA16-RAP1	1897.0210	11.108	51.09 ± 3.76 a	74.79 ± 3.94 a
4	RADA16-RAP2	2761.8655	5.540	87.26 ± 5.04 b	92.68 ± 5.83 b

*Different letters (a–d) represent significant differences at $p<0.05$ per column.

[a] Means half maximal inhibitory concentration; [b] means the peak time of peptides in the ultra performance liquid chromatography (UPLC).

Table 2 GLP-1 secretion after a 60-min STC-1 cells incubation period with peptide or peptide nanogel samples

Group	Sequence	Concentration (μM)	GLP-1 release (pM) *		
			Only peptides or peptide nanogels	With Thermolysin[A]	With DPP-IV[B]
1	RAP1	50	10.17±1.59a	20.08±2.21b	9.55±1.04a
		100	9.95±1.02a	30.45±2.04b	12.76±1.52a
		250	10.04±2.30a	32.63±3.65b	19.46±1.25b
2	RAP2	50	32.88±3.65b	16.57±1.93a	35.69±2.65b
		100	35.69±4.10b	20.25±1.94b	45.65±8.41c
		250	65.62±8.22c	44.62±8.25c	80.11±9.02d
3	RADA16-RAP1	50	9.21±1.52a	13.26±2.00a	10.57±1.52a
		100	11.05±1.55a	18.02±1.98a	12.65±1.87a
		250	11.01±1.50a	22.57±2.35b	14.16±2.23a
4	RADA16-RAP2	50	43.52±8.77c	40.21±6.25c	42.02±3.61c
		100	56.34±7.63c	52.80±5.54c	57.21±4.10c
		250	88.89±7.10d	79.04±6.88d	89.34±7.05d

*Different letters (a–d) represent significant differences at $p<0.05$.

[A] Means one of the protease from *Geobacillus stearot thermophilus*; [B] means the abbreviation for dipeptidyl peptidase

Figure 1

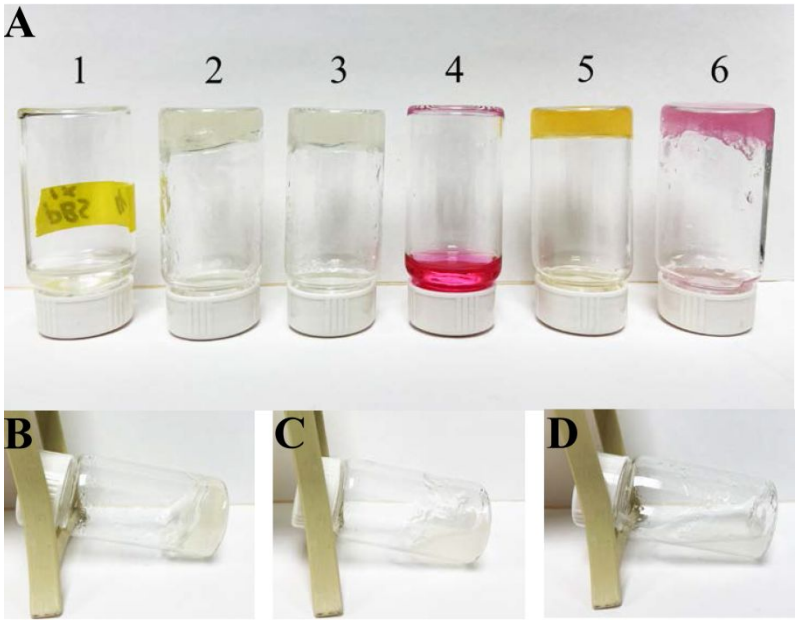
A
1
2
3
4
5
6
B
C
D

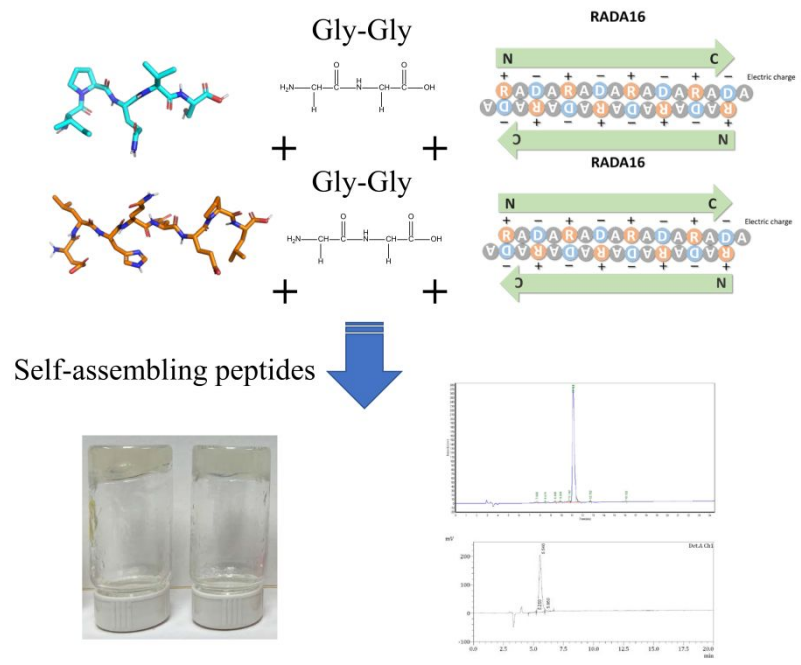
E
Gly-Gly
Gly-Gly
RADA16
RADA16
Electric charge
Electric charge
Self-assembling peptides

Figure 2

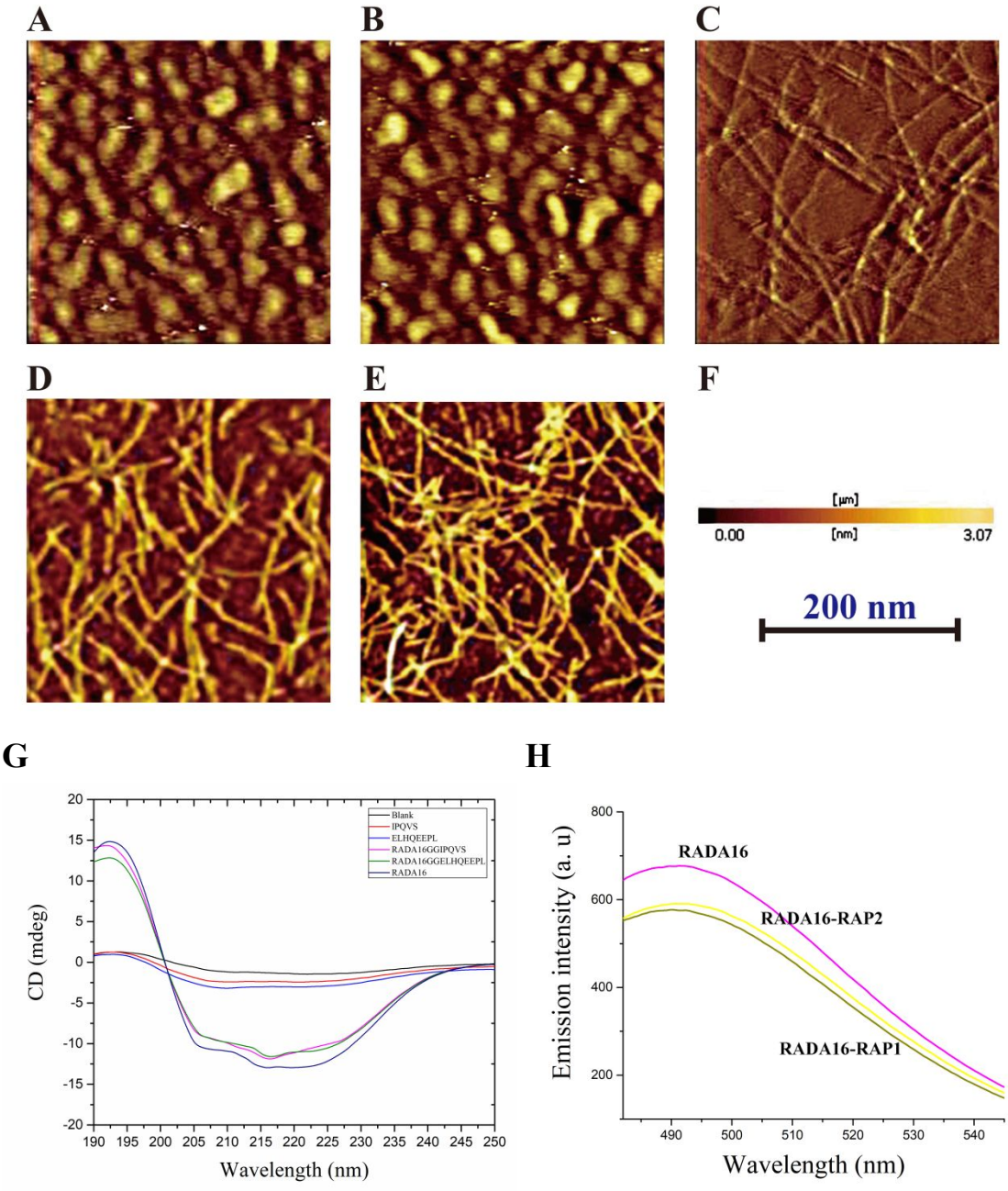
A
B
C
D
E
F
[μm]
0.00
[nm]
3.07
200 nm
G
CD (mdeg)
Wavelength (nm)
Blank
IPQVS
ELHQEEPL
RADA16GGIPQVS
RADA16GGELHQEEPL
RADA16
H
Emission intensity (a. u)
Wavelength (nm)
RADA16
RADA16-RAP2
RADA16-RAP1

Figure 3

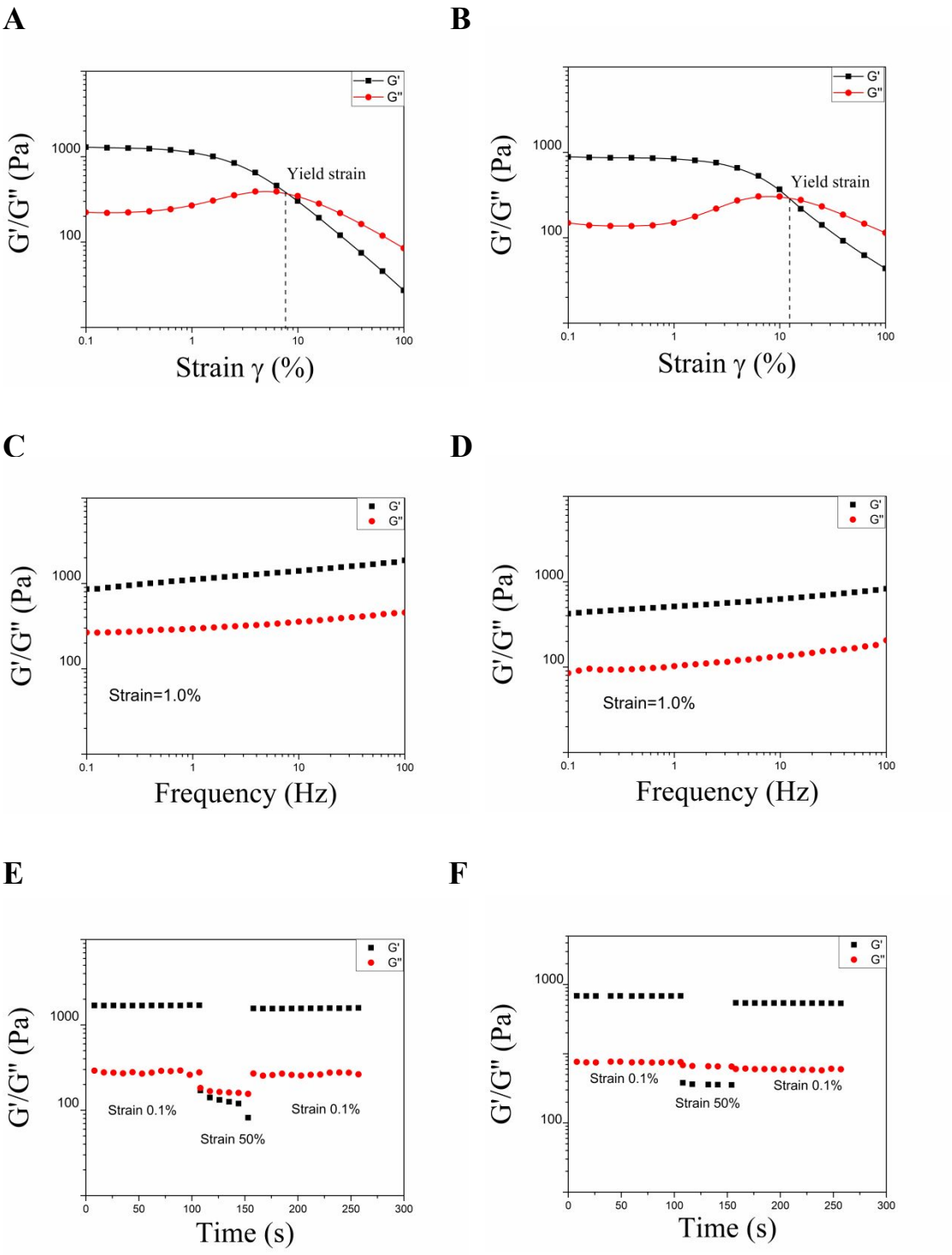
A
B
C
D
E
F
G'
G"
G'/G" (Pa)
Yield strain
Strain γ (%)
Strain=1.0%
Frequency (Hz)
Strain 0.1%
Strain 50%
Time (s)

Figure 4

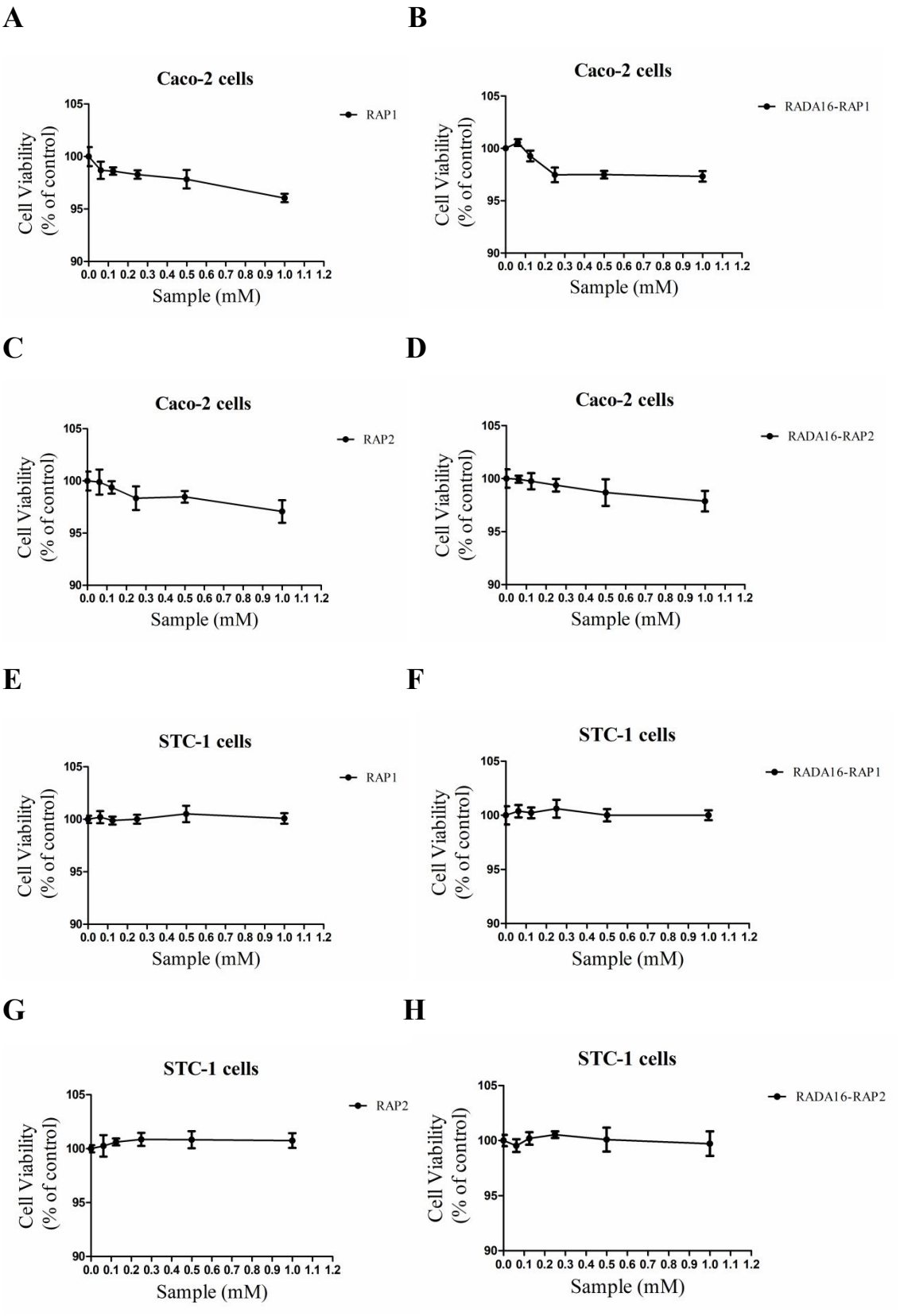
A
Caco-2 cells
RAP1
Cell Viability (% of control)
Sample (mM)
B
Caco-2 cells
RADA16-RAP1
Cell Viability (% of control)
Sample (mM)
C
Caco-2 cells
RAP2
Cell Viability (% of control)
Sample (mM)
D
Caco-2 cells
RADA16-RAP2
Cell Viability (% of control)
Sample (mM)
E
STC-1 cells
RAP1
Cell Viability (% of control)
Sample (mM)
F
STC-1 cells
RADA16-RAP1
Cell Viability (% of control)
Sample (mM)
G
STC-1 cells
RAP2
Cell Viability (% of control)
Sample (mM)
H
STC-1 cells
RADA16-RAP2
Cell Viability (% of control)
Sample (mM)

Figure 5

A

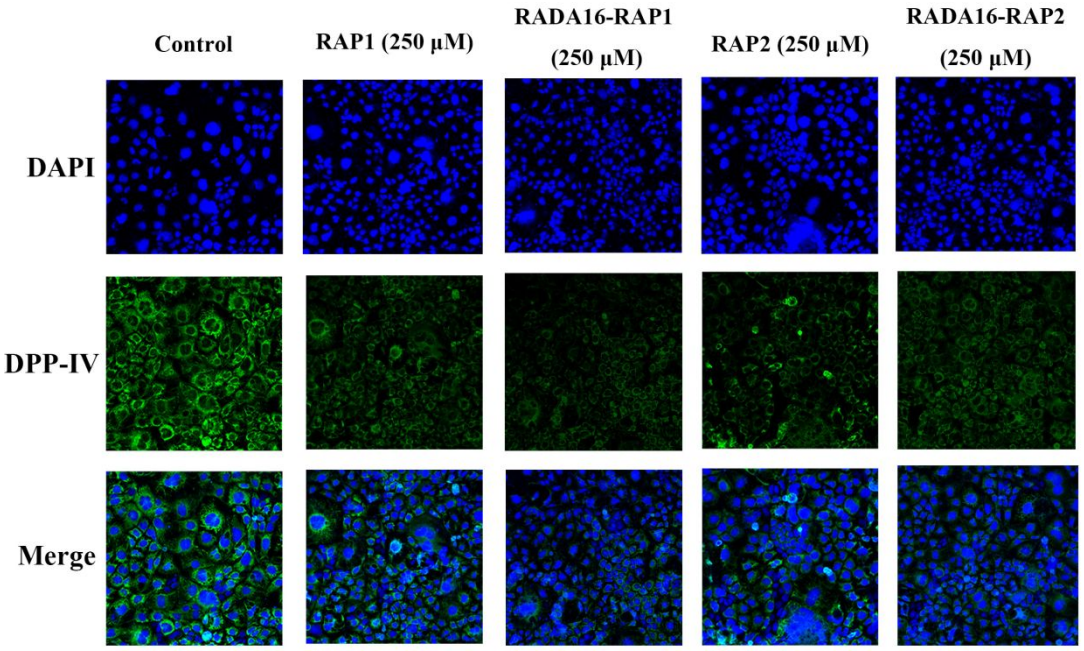
Control
RAP1 (250 μM)
RADA16-RAP1 (250 μM)
RAP2 (250 μM)
RADA16-RAP2 (250 μM)
DAPI
DPP-IV
Merge

B

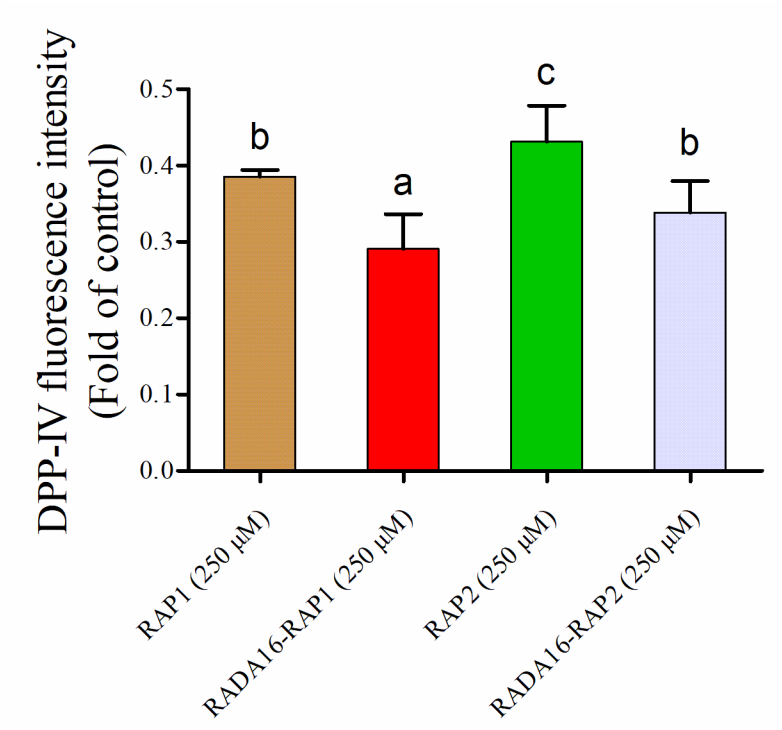
DPP-IV fluorescence intensity (Fold of control)
0.0
0.1
0.2
0.3
0.4
0.5
b
a
c
b
RAP1 (250 μM)
RADA16-RAP1 (250 μM)
RAP2 (250 μM)
RADA16-RAP2 (250 μM)

Figure 6

A

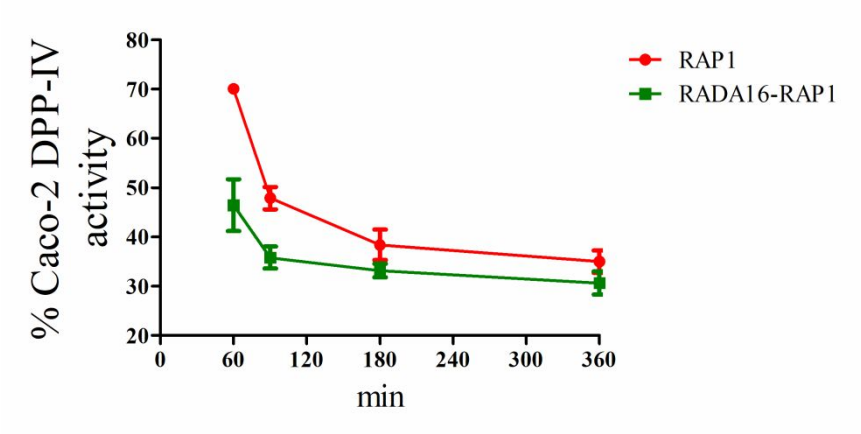
% Caco-2 DPP-IV activity
80
70
60
50
40
30
20
0
60
120
180
240
300
360
min
RAP1
RADA16-RAP1

B

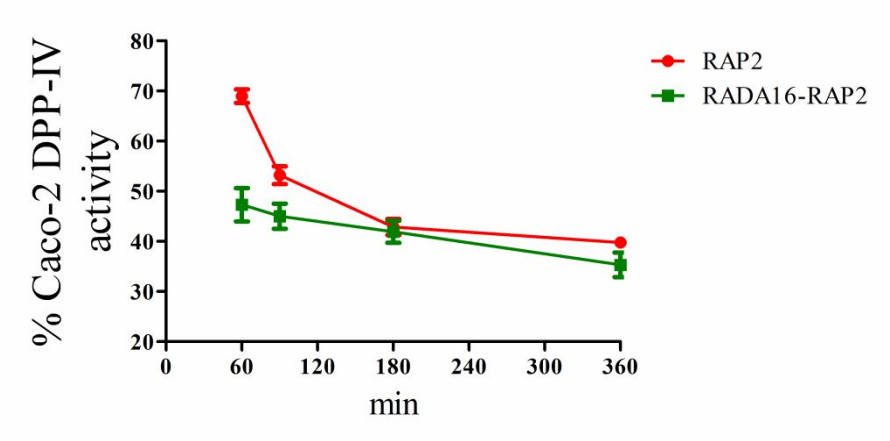
% Caco-2 DPP-IV activity
80
70
60
50
40
30
20
0
60
120
180
240
300
360
min
RAP2
RADA16-RAP2

Figure 7

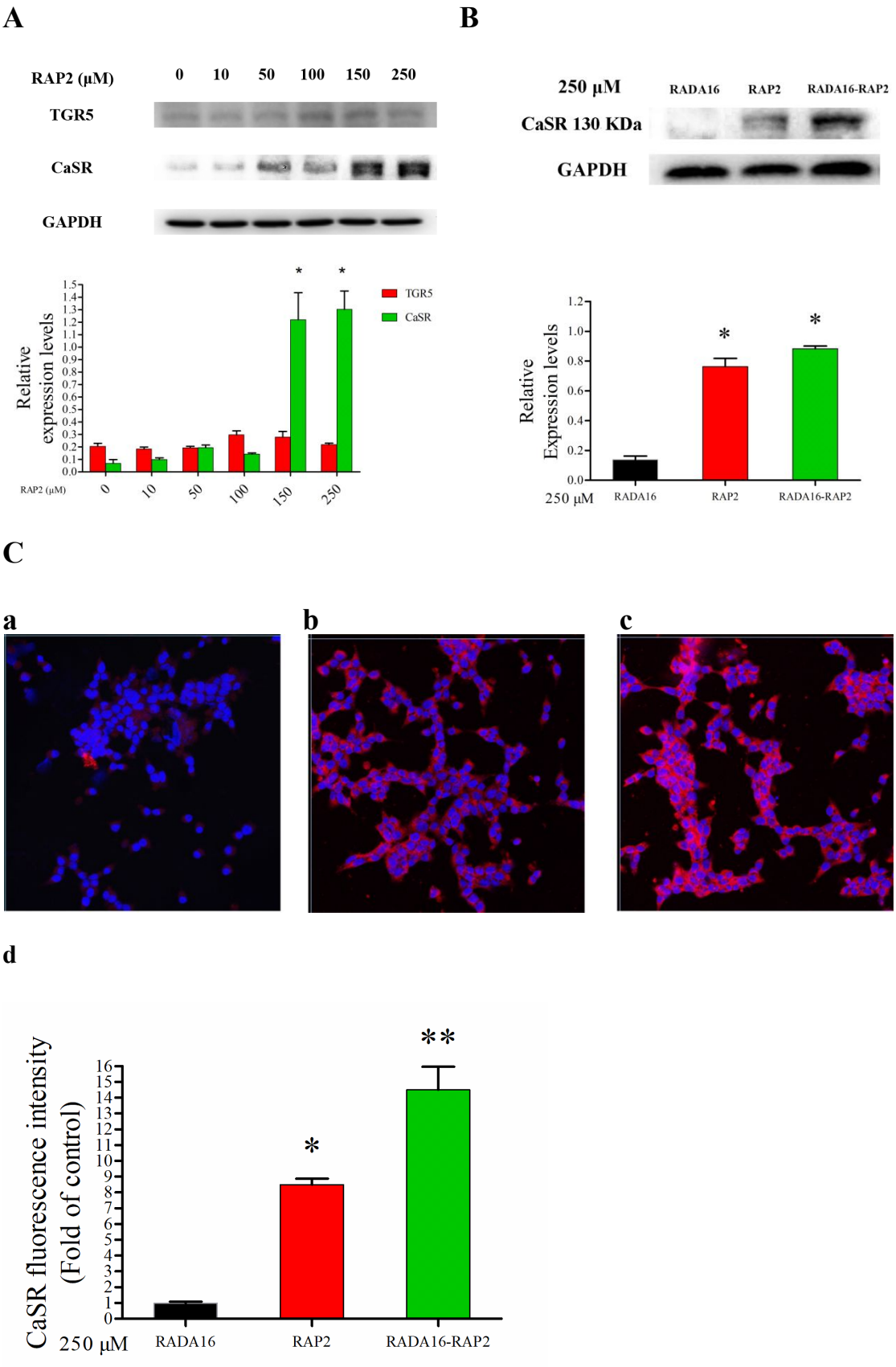
A
RAP2 (μM)
0
10
50
100
150
250
TGR5
CaSR
GAPDH
Relative expression levels
TGR5
CaSR
RAP2 (μM)
B
250 μM
RADA16
RAP2
RADA16-RAP2
CaSR 130 KDa
GAPDH
Relative Expression levels
250 μM
C
a
b
c
d
CaSR fluorescence intensity (Fold of control)
250 μM
RADA16
RAP2
RADA16-RAP2

Figure 8

A

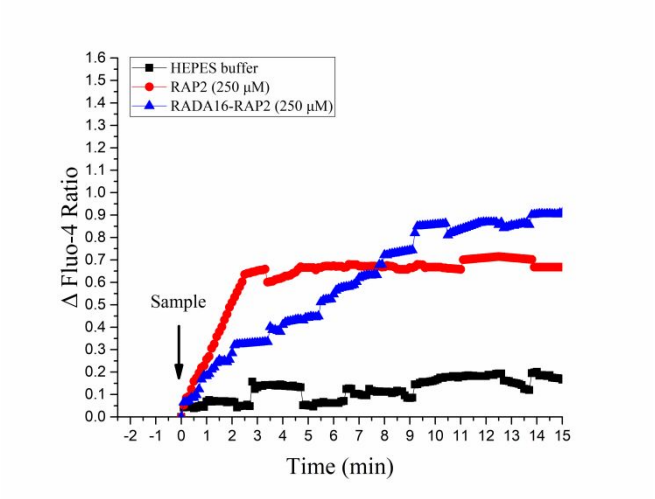
HEPES buffer
RAP2 (250 μM)
RADA16-RAP2 (250 μM)
Δ Fluo-4 Ratio
Sample
Time (min)

B

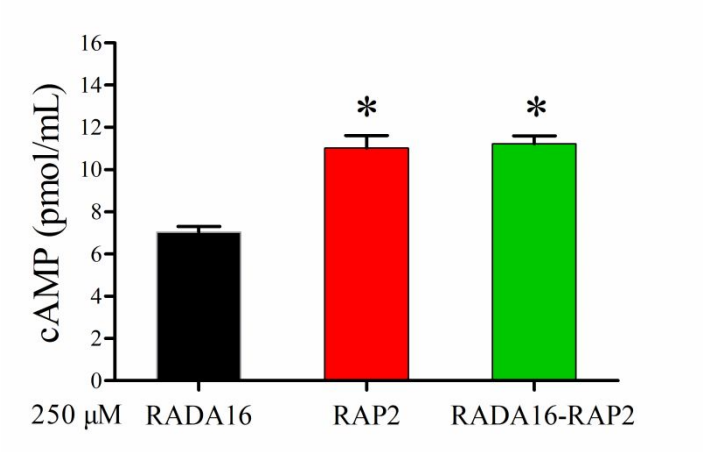
cAMP (pmol/mL)
*
*
250 μM
RADA16
RAP2
RADA16-RAP2